

# Concurrent Transmissions in IR-UWB Networks: an Experimental Validation

James Colli-Vignarelli<sup>†\*</sup> Jérôme Vernez<sup>#</sup> Ruben Merz<sup>‡</sup>  
Catherine Dehollain<sup>†</sup> Stephan Robert<sup>#</sup> Jean-Yves Le Boudec<sup>\*</sup>

<sup>†</sup> EPFL, School of Engineering, <sup>\*</sup> EPFL, School of Computer and Communication Sciences,

<sup>‡</sup> Deutsche Telekom Laboratories, TU Berlin, <sup>#</sup> HEIG-VD

{james.colli-vignarelli, catherine.dehollain}@epfl.ch, {ruben.merz}@telekom.de,

{jean-yves.leboudec}@epfl.ch, {jerome.vernez, stephan.robert}@heig-vd.ch

## Abstract—

We experimentally demonstrate and validate that concurrent and parallel transmissions are feasible for low data-rate impulse-radio ultra-wide band (IR-UWB) physical layers. The optimal organization for a low data-rate IR-UWB network is to allow for concurrent transmissions at the link layer, and to use interference mitigation techniques at the physical layer. In fact, even low data-rate IR-UWB physical layers can suffer from multi-user interference (MUI), especially in near-far scenarios. However, the practical feasibility of such a design has yet to be experimentally tested and validated. Therefore, we perform an experimental validation with a packet-based, low data-rate IR-UWB physical layer testbed. Our results clearly demonstrate that concurrent IR-UWB transmissions are possible. This shows that completely uncoordinated low data-rate IR-UWB networks are feasible. We also demonstrate that, in the presence of MUI, an interference mitigation scheme at the physical layer is indeed necessary. Because it is the first component for the proper reception of a packet, we focus on packet detection and timing acquisition. We show that a traditional scheme is not robust against multi-user interference, and prevents concurrent transmissions. On the contrary, a scheme designed to take MUI into account, even with a very simple interference mitigation scheme, allows for concurrent transmissions, even in strong near-far scenarios.

## I. INTRODUCTION

An impulse-radio ultra-wide band (IR-UWB) physical layer makes use of ultra-short duration pulses to produce extremely wide bandwidth signals [1]. IR-UWB physical layers exhibit several distinctive features. The large bandwidth of UWB radios, typically on the order of the gigahertz, allows for the resolution of the multipath components of the propagation channel [2]. This property, combined with the use of a proper radio receiver, offers a great resistance to multipath fading that usually plagues narrowband radios. The wide bandwidth also allows for multiple-access and provides robustness to interference. The large number of degrees of freedom available can be shared by several communications. In practice, time-hopping provides multiple-access capabilities [1]. In a *low data-rate* setting, time-hopping allows *a priori* for many asynchronous and concurrent transmissions with few interferences

The work presented in this paper was supported (in part) by the National Competence Center in Research on Mobile Information and Communication Systems (NCCR-MICS), a center supported by the Swiss National Science Foundation under grant number 5005-67322, and by CTI contract No7109.2;1 ESPP-ES

between simultaneous transmissions. But, as we explain later in this paper, concurrent transmissions require the presence of interference mitigation functionalities at the physical layer. Another advantage of IR-UWB radios is high precision ranging [3], with a potential for centimeter accuracy in indoor environments. Hence, IR-UWB physical layers may provide both robust communication and ranging capabilities for dense and low data-rate wireless network scenarios.

The properties of UWB physical layers are very different than those of narrowband physical layers. Consequently, the design rules and the architecture of a network composed of IR-UWB nodes are fundamentally different than those for narrowband wireless networks [4], [5], [6]. Narrowband networks need exclusion protocols and power control. On the contrary, for low data-rate IR-UWB networks, the optimal network organization is not to use any exclusion protocols, nor power control [4] (see also [7] regarding the absence of power control). Rather, concurrent transmissions should be allowed at the link layer, rate adaptation used for interference management and an interference mitigation scheme (see [8], [9] and the references therein) used at the physical layer. Indeed, even in a low data-rate setting, an IR-UWB physical layer can suffer from multi-user interference (MUI), especially in near-far scenarios [5]. Essentially, allowing for a bit of complexity at the physical layer allows for a completely uncoordinated network design [6]. Protocols that implement all [5] or parts [10] of the above design principles outperform protocols that use exclusion or power control.

However, the practical feasibility of such a design has yet to be experimentally tested and validated. In fact, all the results previously mentioned have been obtained through theoretical analysis and numerical simulations. Therefore, the contribution of this paper is an experimental validation with a packet-based IR-UWB hardware testbed that concurrent IR-UWB transmissions are possible in a low data-rate setting. In particular, we focus on packet detection and timing acquisition: We show experimentally that for timing acquisition a traditional scheme is not robust enough against multi-user interference, and prevents concurrent transmissions. On the contrary, a scheme designed to take MUI into account [11], even with a very simple interference mitigation scheme, allows for concurrent transmissions, even in strong near-far scenar-

ios, and outperforms a traditional scheme. In the presence of MUI, an interference mitigation scheme at the physical layer is indeed necessary. Our results do not demonstrate a completely working uncoordinated IR-UWB network because our testbed consists of one receiver and several transmitters. Also, we implement a robust packet detection and timing acquisition but not yet a robust demodulation and decoding. Our results in Section III show that a robust demodulation and decoding is definitely required too. This is scheduled for future work. However, our results demonstrate functional parallel and asynchronous IR-UWB transmissions and the feasibility of completely uncoordinated low data-rate IR-UWB networks.

Note that the primary objective of our experimental hardware testbed is extensibility, modularity and flexibility. We want to be able to easily exchange components in the RF chain. We want full access and control of the parameters of the physical layer, and we want to easily implement and test new algorithms at the receiver. For instance, either by programming an FPGA for real-time processing, or by capturing signal traces that can be then used offline with an algorithm implemented in a high-level programming language. Challenges like low power consumption or integration are definitely important but are not primary objectives. This is why most of the RF elements are either off-the-shelf components or are built with discrete-components.

The remainder of this paper is organized as follows: in Section II, we describe the experimental system model of our testbed and the algorithms used along with some important assumptions and limitations of our hardware. We present the results of our experimental performance evaluation in Section III. We conclude the paper in Section IV.

## II. EXPERIMENTAL SYSTEM MODEL AND ASSUMPTIONS

Our experimental setup comprises several transmitters and one receiver (we use two transmitters in Section III for our experiments).

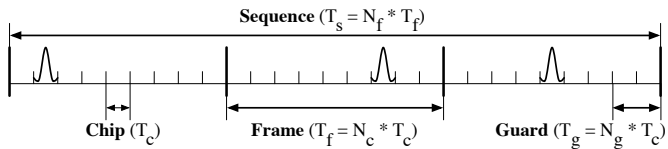


Fig. 1. Classic IR-UWB signal [1] and its parameters:  $T_c$  is the duration of a chip,  $T_f = N_c T_c$  is the duration of a frame and  $T_s = N_f T_f$  is the duration of a sequence.  $T_g = N_g T_c$  is guard time used to prevent ISI.

The physical layer signal generated by each transmitter is a classic IR-UWB signal with time-hopping (TH) as in [1] (see Figure 1): time is divided into frames of duration  $T_f$  and there is one pulse transmitted per frame. Because the pulses are sent infrequently, several transmitters can share the medium concurrently. However, the transmission time of each pulse is randomized to avoid catastrophic collisions [1]. Hence, a frame is further subdivided into  $N_c$  non-overlapping *chips*; for each frame, these chips define the possible locations for the transmission of a pulse. To avoid inter-symbol interference (ISI) due to the multipath propagation channel, a guard time reduces the number of effective available positions by  $N_g$

chips to  $N_c - N_g$ . At last, a sequence is subdivided by  $N_f$  frames.

A so-called pseudo-random time-hopping sequence (THS) of integers uniformly distributed in  $[0, N_c - N_g - 1]$  indicates which position to choose in each frame for the transmission of a pulse. Hence, each transmitter has its own THS, which is independently generated. Information is transmitted thanks to binary pulse position modulation (BPPM), where the position of a pulse carrying a one is shifted by a duration  $T_m$  and the position of a pulse carrying a zero is left unchanged. More formally, the baseband IR-UWB signal with BPPM of the  $n$ -th transmitter is

$$s^{(n)}(t) = \sum_i p(t - iT_f - c_i^{(n)}T_c - d_i^{(n)}T_m) \quad (1)$$

where  $p(t)$  is a pulse,  $c_i^{(n)}$  is an element of the THS of transmitter  $n$  and  $d_i^{(n)} \in \{0, 1\}$  is an information-bearing bit.

In practice, the pulses of the IR-UWB signal generated by our transmitters are simply square pulses of duration  $T_p$  up-converted at  $f_c$ . For time-hopping, for complexity reasons, we do not generate a continuous stream of time-hopping positions. Instead, for each transmitter, we generate a sequence of length  $N_f$  of time-hopping positions and use this sequence repeatedly i.e.  $c_i^{(n)} = c_{i+N_f}^{(n)}$ .

Our experimental system is packet based (see Figure 2). Prior to a payload of length  $L_{pay}$  pulse (or equivalently  $L_{pay}$  bit because of the binary modulation), there is a preamble of length  $L_{pre}$  followed by a so-called preamble delimiter of length  $L_{del}$ . The preamble delimiter is used to detect the beginning of the payload once timing acquisition is achieved. Notice that thanks to time-hopping, each transmitter has its own distinct preamble delimiter. Hence, a receiver can detect and acquire the timing of the packet from a given transmitter while another transmitter is active.

$L_{pre}$ ( $32 * N_s$ )	$L_{del}$ ( $8 * N_s$ )	$L_{pay}$ (127 bytes)
Preamble	Preamble delimiter	Payload (Binary Pulse Position Modulation)

Fig. 2. The structure of the packet sent by the transmitter of interest is loosely based on the IEEE 802.15a standard [12]. It contains three parts: (1) a preamble for packet detection and timing acquisition, (2) a preamble delimiter is used to detect the beginning of the payload and (3) the payload.

Our system is completely asynchronous. There is no global synchronization between the transmitters and the receiver. Hence, at the receiver side, the first operation is packet detection and timing acquisition [13]. We implement two possible algorithms: (1) a conventional correlation based algorithm [14] and (2) a multi-user (MUI) robust algorithm [11]. Both algorithms are correlation based: the received signal is continuously correlated with a template. The correlation  $\Phi$  of the received signal with the template is the sum of several individual correlations with a template corresponding to a received pulse i.e.

$$\Phi = \sum_{i=0}^{L_T-1} \Phi_i \quad (2)$$

where  $\Phi_i$  is the  $i$ -th individual correlation result and  $L_T$  is the length of the template. However, the algorithm in [11] uses a thresholding-based interference mitigation mechanism (see [8], [9] and the references therein): instead of summing the individual correlation, the algorithm in [11] applies a hard decision on the output of each individual correlation, i.e. (2) becomes

$$\Phi = \sum_{i=0}^{L_T-1} 1_{\{\Phi_i \geq \nu\}} \quad (3)$$

This thresholding operation prevents spurious strong correlation outputs, essentially due to near-far interferers, that may completely blind the presence of a valid transmitter. As shown by simulations in [11] and experimentally in Section III, the robust algorithm allows for successful timing acquisitions in the presence of MUI. A conventional algorithm is not sufficient.

A detailed description of both algorithms lies outside the scope of this article. Still, in our implementation, both algorithms bypass coarse timing acquisition and perform directly a fine timing acquisition (they are performed in the digital domain). Once the fine timing acquisition is achieved, a verification phase follows. The initial timing acquisition is declared successful if  $\Phi > \sigma_1$ . The verification phase is declared successful if for  $N_v$  subsequent correlations, we have  $\Phi > \sigma_2$ . If the verification phase is successful, the receiver begins to search for the preamble delimiter. If successful, the receiver can start the demodulation of the payload.

For the demodulation, we currently perform energy detection: the decision rule compares the energy contained at the two possible locations for a zero or a one [14]. The energy at each position is gathered over a duration  $T_{int}$ . At this moment, we do not have any error correction code. We use energy detection because of its simplicity and also because we can avoid any channel estimation. In practice, after band-pass filtering and a low-noise amplification, our receiver performs an IQ down-conversion. Even though we perform energy detection, we use a mixer for the demodulation for extensibility reasons: we want to be able to implement coherent processing in addition to energy detection. The signal after down-conversion is fed to an analog to digital converter (ADC) running at  $f_s$ . The ADC is coupled to an FPGA. The samples are then directly moved into a large DRAM on the FPGA and stored. The remaining operations, packet detection and timing acquisition and demodulation, are all performed in the digital domain. For instance, for energy detection, the integration over a duration  $T_{int}$  is replaced by a summation of  $N_{int}$  samples where  $N_{int} = T_{int} \cdot f_s$ . These operations are also all performed offline after the signal trace contained in the DRAM is offloaded to a PC. For instance, our ADC is running at 2 GS/s with an 8 bits resolution and we have 512 Mbyte of DRAM. We can store a signal trace of about 0.256 seconds. In our setting, this is sufficient to capture one or more packets and process them offline. We could use the FPGA to process the signal in real-time. However, an offline processing, although time consuming, allows for a greater flexibility. Real-time processing is scheduled for future work.

An overview of our experimental testbed with its characteristics is shown in Figure 3.

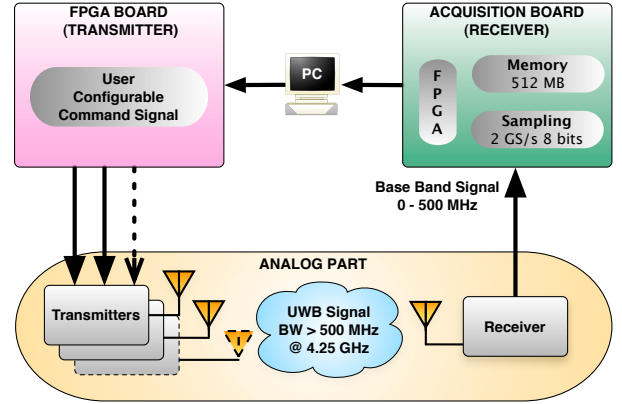


Fig. 3. Overview of the testbed: an FPGA board controls the transmitters with the desired signal characteristics. The receiver amplifies, filters and down-converts the received signal to the base band. The acquisition board of the receiver samples the base band signal and stores this signal trace in DRAM on another FPGA. The signal trace is later offloaded to a PC for offline processing.

### III. PERFORMANCE EVALUATION

#### A. Measurements Settings

We consider three different scenarios for our experimental performance evaluation. First, a *single user* scenario (scenario A, Figure 4(a)): one transmitter located at distance  $L$  of the receiver. We use Scenario A to validate our implementation and to obtain reference results. For the second scenario, (scenario B, a *equal power* topology, Figure 4(b)), we have an additional interfering transmitter also at distance  $L$  from the receiver. Hence, the received power from the transmitter of interest and from the interfering transmitter is roughly identical. For the third scenario (scenario C, a *near-far* topology, Figure 4(c)), the additional interfering transmitter is positioned in a near-far situation at a distance  $L_{nf} < L$  from the receiver. The received power from the interfering transmitter is much higher than the power received from the transmitter of interest. This is a typical sensor networks or ad hoc network situation. We perform all experiments with line-of-sight (LOS) propagation. We consider  $L = 1, 3, 6$  meters and  $L_{nf} = 0.2$  meter.

Our main performance metrics is the percentage of achieved packet detection and timing acquisition ( $A_{PDTA}$ ). A packet detection and timing acquisition is declared to be achieved if a preamble delimiter is detected. This does not ensure that packet detection and timing acquisition was absolutely successful. For this, we would need a time reference for the received packet in order to compare with the timing acquired by our timing acquisition algorithm. But, for each packet where timing acquisition was achieved, we can however verify the BER of the payload. We observed during trial runs that if timing acquisition was incorrect, the BER was generally above 0.3 (even with MUI). Hence, for each packet where timing acquisition is achieved, we always compute the BER of this packet. If the BER is above a verification threshold  $\gamma$ , we declare that timing acquisition failed.

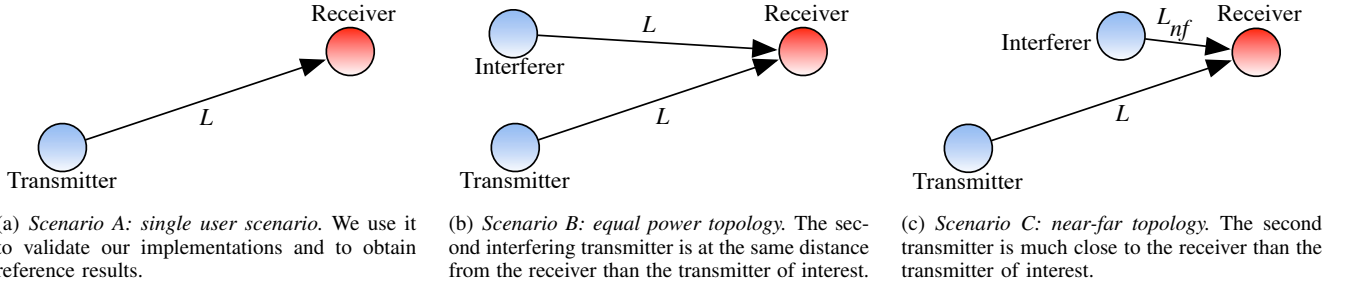


Fig. 4. The three topologies used for our experiments: a single user scenario, an equal power interference scenario and a near-far interference scenario.

Two other performance metrics that we also consider are the packet error rate (PER) and the bit error rate (BER); both of them are computed with payload where timing acquisition was achieved.

The transmitter in interest sends packets, whereas the interfering transmitter sends a continuous signal with a random time-hopping code. To obtain statistically meaningful results we transmit 10000 packets per experiment run. As explained in Section II, for each packet transmission, we first store the received signal in the DRAM of the FPGA. We then transfer the signal trace to a PC for offline processing. We perform all the processing with Matlab where we extensively use external functions written in C. Still, a typical 10000 packets experiment run lasts around 20 hours. Also, before each experiment run, we always carefully recalibrate the hardware: We verify and adjust the power spectral density of our signal to make sure it is FCC compliant; we adjust the timing acquisition thresholds; We set the range of the ADC to avoid any clipping on the strongest received signal.

These last two operations, threshold setting and range calibration are normally done automatically by estimating the noise variance and by performing automatic gain control (AGC) at the receiver. This is left for future work.

The parameters of the physical layer (see Section II) are assigned to the following values. The IR-UWB signals parameters such that the number of chips and the number of frame are fixed to  $N_c = 128$  chips and to  $N_f = 8$  frames. The  $N_g$  is set to 8 chips. The affecting packets characteristics are set to the values given in the Figure 2;  $L_{pre} = 32 * N_s$ ,  $L_{del} = 8 * N_s$ ,  $L_{pay} = 127$ . With these values, packet duration corresponds to about 1 ms. The timing acquisition algorithms use a template with a pulse's width of 0.5 ns. The initial timing acquisition and verification phase use both thresholds of  $\sigma_1 = 0.625$  and  $\sigma_2 = 0.75$ . These values are the optimal result found by [11]. A summary of these values is given in Table I.

$N_c=128$ chips	$N_g=8$ chips
$N_f=8$ frames	$L_{pre}=32*N_s$
$L_{del}=8*N_s$	$L_{pay}=127$ bytes
$T_p$ template=0.5 ns	$N_v=16$
$\sigma_1=0.625$	$\sigma_2=0.75$

TABLE I  
THE PARAMETERS USED FOR THE EXPERIMENT RUNS.

## B. Measurements Results

For each measurement run the both timing acquisition algorithms are applied (conventional and MUI robust). We noticed that the results found with the conventional correlation based algorithm vary a lot in comparison with the results obtained with the MUI robust algorithm. Ones which are reported here are the ones which gave the best results for the conventional method. Figure 5 shows us the percentage of achieved packet detection and timing acquisition  $APD_{DTA}$ . Two other performance metrics, the PER and the BER are reported in Tables II and III.

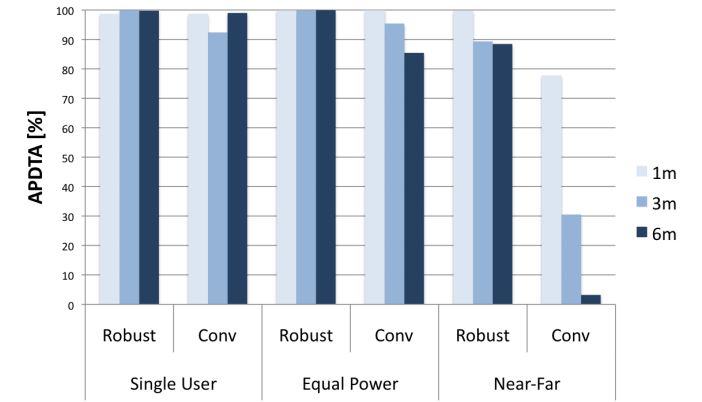


Fig. 5. Measurement results of achieved packet detection and timing acquisition ( $APD_{DTA}$ ) for two timing acquisition algorithms, Robust (multi-user robust algorithm) and Conv (conventional correlation based algorithm), in three scenarios : *single user*, *equal power* and *near-far*, where in each case the transmitter lies at three different distances (1, 3 and 6 m). The *single user* uses one transmitter in order to simulate the ideal case, the *equal power* involves the transmitter and interferer at equal distance in order to evaluate interference robustness without power consideration and finally, the *near-far* scenario which shows the robustness in the worst case. There are 10000 transmitted packets for each run.

Figure 5 shows that the MUI robust algorithm performs better than the conventional correlation based algorithm, especially when the distance between the transmitter and the receiver increases. Interestingly, we notice that both algorithms give almost similarity results in the two first scenarios (*single user* and *equal power*). However in the third one (*near-far*), the conventional algorithm yields a low  $APD_{DTA}$  most of the time. The MUI robust algorithm is far more efficient in the *near-far* topology where the interference are the most marked.

In the *single user* scenario we can see that the PER is relatively low for both methods. In the two other scenarios it is

PER [%]	Single User		Equal Power		Near-Far	
	ROB	CONV	ROB	CONV	ROB	CONV
1m	1.27	1.27	39.36	39.27	65.98	72.65
3m	0.0	7.62	37.77	40.58	79.47	91.44
6m	0.26	1.01	54.71	61.47	70.43	98.73

TABLE II  
MEASUREMENT RESULTS OF PACKET ERROR RATE (PER)

BER [%]	Single User		Equal Power		Near-Far	
	ROB	CONV	ROB	CONV	ROB	CONV
1m	0.0	0.0	0.49	0.48	2.35	2.40
3m	0.0	0.0	0.28	0.27	3.76	4.16
6m	0.004	0.004	0.85	0.85	4.42	3.95

TABLE III  
MEASUREMENT RESULTS OF BIT ERROR RATE (BER)

relatively high in contrast. This is due to the fact that a packet is considered as corrupted when only one bit is erroneous. Be it reminded, no error correction or demodulation optimization are used.

As expected the bit error rate (BER) increases with the distance between the transmitter and the receiver. It should be noted here that when the  $A_{PDTA}$  has failed, the BER is not considered. That explains why it can be higher with the MUI robust method than with conventional method.

Additional observations have been made during the trial phase. We observed for instance that the BER is lower when  $N_c$  is higher and  $A_{PDTA}$  which is better when  $N_f$  is higher for both algorithms.

### C. Validity of our Results

To validate our results, two main points have to be considered; our non-perfect hardware and the manually tuned of thresholds. First of all, we have notice that the conventional algorithm's  $A_{PDTA}$  varies a lot from one experiment to another. We expect that the results of the conventional algorithm is very sensitive to the environment in general. The fact that the laboratory where measurements are performed is not immune to electromagnetic radiations at all have to be considered. However the main cause of these variations comes from our hardware. The pulses amplitude is not always constant as it should be, especially because of the imperfections of the oscillator, which is very dependent on the power supply stability and on temperature variations. Multi-paths also strongly affect the pulse's amplitude as well as the hardware. We did notice for instance that the variation of the pulse's amplitude has a relatively big impact on the conventional algorithm performance. Nevertheless we have shown that the MUI robust method gives good results in spite of imperfect hardware.

Secondly, the choice of timing acquisition thresholds ( $\nu$ ) potentially influences the results a lot. The timing acquisition threshold of both algorithms is separately set, depending on the received power (in practice, we have to decrease the threshold as a function of the distance to obtain the best results). For the scenarios and distances of our measurement sets, the MUI robust algorithm timing acquisition threshold does not have

to be tuned a lot. The situation is very different with the conventional algorithm where the timing acquisition threshold has to be adjusted for scenarios A and B (In scenario C, it is constant because the interference is also constant in power). It is tuned manually and set after a certain number of trials. Therefore this way of doing things does not allow us to strictly compare results for both methods since needs many manual adjustments. However the overall trends of the results obtained is validate by the multiple measurement runs performed. Eventually, we remember that the MUI robust method better manages power differences, since the conventional timing acquisition threshold does have to be more tuned.

## IV. CONCLUSION

We experimentally demonstrated that concurrent transmissions are feasible in low data-rate IR-UWB networks. We also showed that interference mitigation techniques are indeed necessary at the physical layer. Because it is the first component for the reception of a packet, we focused on packet detection and timing acquisition.

For future work, we plan to improve the hardware receiver, to implement a better demodulation of the data payload, to implement a bit control and to add an automatic gain control (AGC) at the receiver. Then we could make new measurement sets in clean environment with more transmitters.

## V. ACKNOWLEDGEMENTS

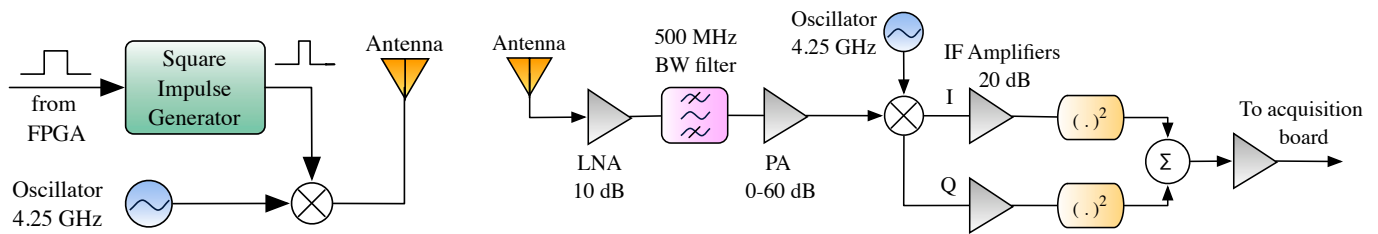
The authors would like to acknowledge Jean-François Zürcher, Gabriela Quintero Diaz de Leon, Anja Skriverik, Yasmine Akhertouz Moreno, Prakash Thoppay Egambaram, as well as the ACI and ACORT team from EPFL, STI, Raymond Knopp from Eurecom and Robin Scheibler and Manuel Flury from EPFL, IC.

## APPENDIX

### OVERVIEW OF THE IR-UWB TESTBED

In this section, we give a brief overview of our IR-UWB testbed (see Figure 3). On the transmitter side, we can generate several concurrent IR-UWB signals with a bandwidth of at least 500 MHz. For this purpose, an FPGA creates several command signals that each drives an IR-UWB transmitter. Each command signal is a simple low voltage digitally controlled impedance (LVDCI) signal where rising edges correspond to a pulse transmission. The maximum clock frequency of our FPGA is 166 MHz. This translates to a minimum chip duration  $T_c$  of 6 ns. Hence, we have the ability to fully control each parameter of the transmitted signal (see Equation (1)) and can be configured by the computer through registers.

The FPGA is connected to each IR-UWB transmitter through a Micro DB connector. Hence, our analog IR-UWB transmitter was built to be robust to distortions of the command signal. Its architecture is depicted in Figure 6(a): An integrated PLL sine wave oscillator running at  $f_c = 4.25$  GHz is connected to the antenna through a mixer. The mixer behaves like a switch when driven by a square signal. The output of the PLL is amplified before the mixer. An important part of the transmitter is the square impulse generator. Indeed, driven by



(a) The impulse generator creates an impulse of 2 ns driven by the FPGA. The mixer, then, switches on and off the oscillator sine wave and produces the IR-UWB signal.

(b) The received signal is amplified and filtered before being down-converted by a IQ-mixer. The mixer has its local oscillator frequency at 4.25 GHz. The baseband signal is amplified and sent to the FPGA for sampling.

Fig. 6. Operating principle of the whole RF part.

a possibly degraded FPGA command signal, it must reliably generate short squared impulses of 2 ns to drive the mixer. The duration of the pulse can be finely tuned with a trimmer.

The receiver is a classic direct-conversion circuit (see Figure 6(b)). The signal from the antenna is amplified by a LNA followed by a power amplifier and then down-converted with an IQ mixer driven by a 4.25 GHz sine wave. The signal is additionally band-pass filtered inside the LNA. The design of our antennas is described in [15]. Most of our receiver is built around discrete components with off-the-shelf integrated circuits. Hence, we carefully designed them to avoid any undesired interferences and spurious coupling between components. We made sure to shield whenever necessary to preserve the integrity of the received signal.

The list of components used for the testbed is in Table IV.

FPGA	Virtex II Pro XC2VP70, Xilinx
Acquisition board	AC-240 (512 MB SDRAM), Acqiris
PLL oscillator	PCA 4260C-LF, Z-Comm
Switching mixer	HMC128, Hittite Corporation
LNA transistor	NESG2030M04, NEC
Power amplifier	MMIC MGA-85563, Agilent
IQ mixer	HMC525, Hittite Corporation
Squaring mixer	ZLW-11, Mini-Circuits
IF amplifier	ZX60-3018G, Mini-Circuits
Duroid substrate	RO4003B, Rogers Corporation

TABLE IV  
LIST OF COMPONENTS USED FOR THE TESTBED.

## REFERENCES

- [1] R. Scholtz, "Multiple access with time-hopping impulse modulation," in *IEEE Military Communications Conference (MILCOM)*, vol. 2, 1993, pp. 447–450 vol.2.
- [2] M. Z. Win and R. A. Scholtz, "On the robustness of ultra-wide bandwidth signals in dense multipath environments," *IEEE Commun. Lett.*, vol. 2, no. 2, pp. 51–53, 1998.
- [3] S. Gezici, Z. Tian, G. Giannakis, H. Kobayashi, A. Molisch, H. V. Poor, and Z. Sahinoglu, "Localization via ultra-wideband radios: a look at positioning aspects for future sensor networks," *IEEE Signal Process. Mag.*, vol. 22, no. 4, pp. 70–84, July 2005.
- [4] B. Radunovic and J. Y. Le Boudec, "Optimal power control, scheduling and routing in UWB networks," *IEEE J. Sel. Areas Commun.*, vol. 22, no. 7, pp. 1252–1270, September 2004.
- [5] R. Merz, J. Widmer, J.-Y. Le Boudec, and B. Radunovic, "A joint PHY/MAC architecture for low-radiated power TH-UWB wireless ad-hoc networks," *Wireless Commun. and Mobile Comput. J., Special Issue on Ultrawideband (UWB) Communications*, vol. 5, no. 5, pp. 567–580, August 2005.
- [6] B. Radunovic, J.-Y. Le Boudec, and R. Knopp, "Optimal PHY and MAC Protocols for Wide-Band Ad-Hoc Networks," in *Forty-Fifth Annual Allerton Conference*, 2007.
- [7] F. Cuomo, C. Martello, A. Baiocchi, and C. Fabrizio, "Radio resource sharing for ad hoc networking with UWB," *IEEE J. Sel. Areas Commun.*, vol. 20, no. 9, pp. 1722–1732, December 2002.
- [8] M. Flury and J.-Y. Le Boudec, "Interference mitigation by statistical interference modeling in an impulse radio UWB receiver," in *IEEE International Conference on Ultra-Wideband*, September 2006, pp. 393–398.
- [9] J. Mitra and L. Lampe, "Robust detectors for TH IR-UWB systems with multiuser interference," in *Ultra-Wideband, 2007. ICUWB 2007. IEEE International Conference on*, September 2007, pp. 745–750.
- [10] M.-G. Di Benedetto, L. Nardis, M. Junk, and G. Giancola, "(UWB)<sup>2</sup>: Uncoordinated, wireless, baseborn, medium access control for UWB communication networks," *Mobile Networks and Applications*, vol. 10, no. 5, October 2005.
- [11] A. El Fawal and J.-Y. Le Boudec, "A robust signal detection method for ultra wide band (UWB) networks with uncontrolled interference," *IEEE Trans. Microw. Theory Tech.*, vol. 54, no. 4, pp. 1769–1781, June 2006.
- [12] IEEE Computer Society, LAN/MAC Standard Committee, "IEEE P802.15.4a/D7 (amendment of IEEE std 802.15.4), part 15.4: Wireless medium access control (MAC) and physical layer (PHY) specifications for low-rate wireless personal area networks," Jan. 2007.
- [13] J. G. Proakis, *Digital Communications*, 4th ed. New York, NY: McGraw-Hill, 2001.
- [14] C. Carbonelli and U. Mengali, "Synchronization algorithms for uwb signals," *IEEE Trans. Commun.*, vol. 54, no. 2, pp. 329–338, 2006.
- [15] G. Quintero Diaz de Leon and A. Skrivervik, "Analysis of UWB antennas for carrier-based UWP impulse radio," in *European Conference on Antennas and Propagation*, November 2007, pp. 1–4.